Theoretical study of $^4I_{13/2} \rightarrow {}^4I_{15/2}$ luminescence quenching by OH for $LaF_3:Er^{3+}$ nanoparticles in solution

2007 J. Phys.: Condens. Matter 19 016202

(http://iopscience.iop.org/0953-8984/19/1/016202)

INSTITUTE OF PHYSICS PUBLISHING JOURNAL OF PHYSICS: CONDENSED MATTER

J. Phys.: Condens. Matter **19** (2007) 016202 (14pp) doi:10.1088/0953-8984/19/1/016202

Theoretical study of $^4I_{13/2} \rightarrow {}^4I_{15/2}$ luminescence quenching by OH for $LaF_3:Er^{3+}$ nanoparticles in solution

L Ning[1], L Lodi[1], M I Trioni[1], R Tubino[1], S Edvardsson[2] and G P Brivio[1]

[1] Dipartimento di Scienza dei Materiali and CNISM, Università degli Studi di Milano-Bicocca, via Cozzi 53, 20125 Milano, Italy
[2] Department of Physical Electronics and Photonics, Mid Sweden University, S-851 70, Sundsvall, Sweden

Received 8 September 2006, in final form 8 November 2006
Published 7 December 2006
Online at stacks.iop.org/JPhysCM/19/016202

Abstract

The processes of $^4I_{13/2} \rightarrow {}^4I_{15/2}$ luminescence quenching by OH vibrations are investigated for $LaF_3:Er^{3+}$ nanoparticles dissolved in solution. The energy transfer (ET) rates, involving the $^4I_{13/2} \rightarrow {}^4I_{15/2}$ transition of Er^{3+} and the first overtone absorption of OH, are estimated. In order to calculate the relevant OH transition matrix elements, a model for the OH vibration in solution is developed with the use of a Morse potential. Various multipole–multipole ET mechanisms are considered and their dependences on the distance between Er^{3+} and OH are studied. Based on these ET mechanisms, the ET rates from an Er^{3+} in the nanoparticle to all the OH in solution are estimated and compared with respect to changes in location of the ion, size of the nanoparticle and OH concentration in solution. The effective $^4I_{13/2} \rightarrow {}^4I_{15/2}$ luminescence decay times that are contributed by all the Er^{3+} in the nanoparticle are then calculated with different Er^{3+} concentrations. The calculations satisfactorily account for experimental observations.

1. Introduction

In recent years there has been a growing interest in the optical behaviour of lanthanide-doped inorganic nanoparticles dissolved in organic solvents [1–5]. The lanthanide ions in these nanoparticles are shielded from the organic surroundings, and as a result the luminescence lifetimes could be orders of magnitude larger than those observed by directly incorporating the lanthanide ions into organic environments [3]. This is especially important for lanthanide ions emitting in the near-infrared, because the energies involved in these transitions are smaller and thus quenching of the luminescence by energy transfer (ET) to high-energy vibrational modes in the solvent is much more pronounced. For example, the $^4I_{13/2} \rightarrow {}^4I_{15/2}$ luminescence of Er^{3+} around 1.53 μm, which is one of the standard telecommunications wavelengths, can be

quenched efficiently by the OH vibrations of water in the solvent, since the energy of the $^4I_{13/2} \rightarrow {}^4I_{15/2}$ transition ($E = 6540\ \text{cm}^{-1}$) is in strong resonance with the first overtone of the OH vibration ($E_0 = 3400\ \text{cm}^{-1}$). A detailed description of such quenching processes requires a detailed knowledge of the electronic structures and transitions of lanthanide ions and of vibrational transitions of the high-energy modes in the solvent. While the former may be obtained by the usual spectroscopic techniques, the latter has shown to constitute a rather difficult problem.

Although the luminescence quenching of lanthanide ions in environments with OH vibrations has been known for decades, theoretical calculations for such ET processes (from lanthanide ions to OH) are rather scarce [6, 7], in contrast to the widely performed theoretical calculations for ET processes between lanthanide ions in inorganic compounds [8–10]. Stavola and Dexter [7] calculated the ET rates involving simultaneous lanthanide electronic and OH vibrational transitions in condensed matter. After deriving the ET formulation along the lines of Förster [11] and Dexter [12], they simplified calculations for the involved lanthanide electronic transitions using the approximations of Kushida [8], and estimated the relevant OH transition matrix elements from the experimentally determined oscillator strengths. They also pointed out that the derived ET formulation was equally applicable to ET processes occurring between the lanthanide ion and OH in aqueous solutions, if the relevant OH transition matrix elements were known.

In the present work we have studied ET processes from the excited $^4I_{13/2}$ manifold of Er^{3+} in LaF_3 nanoparticles to OH vibrations in solution. Recently, the $^4I_{13/2} \rightarrow {}^4I_{15/2}$ luminescence decays for LaF_3:Er^{3+} nanoparticles dissolved in the organic solvent have been measured, and the quenching role of the residual water in the solvent was observed [3]. In order to facilitate the calculation of ET rates, a model for the OH vibration in solution has been developed, by which the OH transition matrix elements have been derived using a Morse potential. At the same time, advantage has been taken of the ET formulation developed in [7] and the well characterized optical properties of Er^{3+} in the LaF_3 crystal [13]. The results of this work, which is focused on the demonstration of ET calculations involving lanthanide electronic transitions in inorganic nanoparticles and OH vibrations in solution, may also act as a reference for the interpretation of the $^4I_{13/2} \rightarrow {}^4I_{15/2}$ luminescence quenching of Er^{3+} by water solution, which is not available in the literature.

This paper is organized as follows. The theoretical background of ET processes between a lanthanide ion and an OH group is presented in section 2. In section 3 the modelling of OH vibration in solution is described and the relevant OH transition matrix elements are derived. The results of the ET calculations are presented and discussed in section 4, with the final conclusions collected in section 5.

2. Theory

The approximate expression for the ET rate between a lanthanide ion and a molecule, which are denoted by centres A and B, respectively, may be expressed as [7]

$$P_{AB} = \frac{2\pi}{\hbar}\left[\frac{1}{\kappa^2}\sum_{k_1k_2}\left[\frac{e^2}{R^{k_1+k_2+1}}\right]^2 \frac{(2k_1+2k_2)!}{(2k_1+1)!(2k_2+1)!}\sum_{q_1,\gamma,\gamma'}\frac{\left|\langle J\gamma\left|D^{k_1}_{q_1}(A)\right|J'\gamma'\rangle\right|^2}{(2J+1)(2J'+1)} \times \sum_{q_2}\left|\langle 00\left|M^{k_2}_{q_2}(B)\right|0n\rangle\right|^2\right]\rho_E \tag{1}$$

where centre A makes an electronic transition and centre B a vibrational one. κ is the high-frequency dielectric constant, which acts as a screening constant for the interaction, and R is

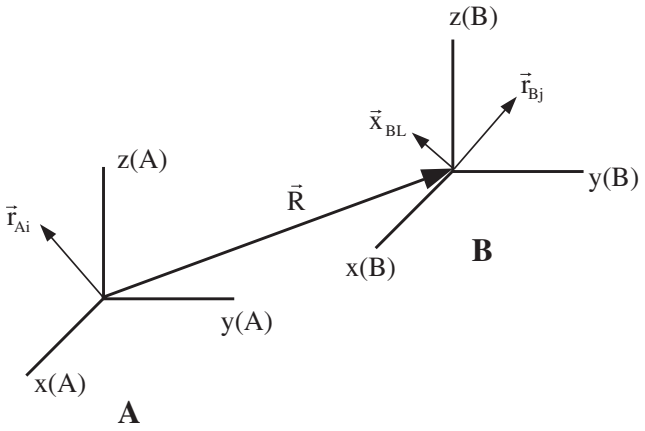

Figure 1. The coordinate system for the two centres A and B.

the separation between centres A and B. The coordinate system for the two centres is shown in figure 1. Both the electron–electron and electron–nuclear interactions between centres A and B have been considered. The electric multipole moment operators in equation (1) are given by

$$D_q^k(A) = \sum_i r_{Ai}^k C_q^k(\theta_i, \phi_i), \tag{2}$$

$$M_q^k(B) = \sum_j r_{Bj}^k C_q^k(\theta_j, \phi_j) - \sum_L Z_L x_{BL}^k C_q^k(\theta_L, \phi_L), \tag{3}$$

with

$$C_q^k(\theta, \phi) = \left(\frac{4\pi}{2k+1}\right)^{1/2} Y_{kq}(\theta, \phi). \tag{4}$$

In these expressions $(r_{Ai}, \theta_i, \phi_i)$ and $(r_{Bj}, \theta_j, \phi_j)$ are the polar coordinates of electrons i and j at centres A and B, respectively, and $(x_{BL}, \theta_L, \phi_L)$ are the coordinates of nucleus L at centre B. They are all measured from their respective centres of mass. Z_L is the atomic number of the Lth nucleus at centre B. The kets $|J\gamma\rangle$ and $|J'\gamma'\rangle$ are the initial and final crystal-field (CF) states of the lanthanide ion (centre A), and the $|0n\rangle$ is the Born–Oppenheimer state of centre B with the index 0 indicating the ground electronic state and the index n the quantum number for the vibrational one. The summation is over $q = -k, \ldots, k$, and the components γ of the initial and final CF levels of the lanthanide ion. The overlap integral ρ_E is defined as [7]

$$\rho_E = \sum_{\gamma\gamma'} \frac{\mathrm{e}^{-E_\gamma/kT}}{Q} \int f_{\gamma\gamma'}(E) F_{00,0n}(E)\, \mathrm{d}E. \tag{5}$$

Here, the integral is over the normalized line-shape functions for the radiative transitions, $|J\gamma\rangle \to |J'\gamma'\rangle$ and $|00\rangle \to |0n\rangle$, of centres A and B, respectively, and represents the density of the energy-conserving states. The Boltzmann factor has been included to account for the thermal distribution of energy among the initial CF levels of the lanthanide ion, and

$$Q \equiv \sum_\gamma \mathrm{e}^{-E_\gamma/kT},$$

is the partition function. Depending on different interaction mechanisms, P_{AB} can be reduced to different formulae as follows:

$$P_{AB}^{dd} = \frac{2\pi}{\hbar}\frac{1}{\kappa^2}\left(\frac{2}{3}\right)\frac{e^4}{R^6}\frac{1}{(2J+1)(2J'+1)}\left[\sum_{\lambda=2,4,6} \Omega_\lambda^{\mathrm{ed}} \left\langle J \left\| U^{(\lambda)} \right\| J' \right\rangle\right]$$

$$\times \left[\sum_q \left|\left\langle 00\left|M_q^1(B)\right|0n\right\rangle\right|^2\right]\rho_E, \tag{6}$$

for the electric dipole–electric dipole interaction, where $\Omega_\lambda^{\mathrm{ed}}$ ($\lambda = 2, 4, 6$) are the 4f–4f intensity parameters without the contribution from the so-called dynamic coupling mechanism of 4f–4f intensities [14], and $\langle J||U^{(\lambda)}||J'\rangle$ are the reduced matrix elements of the unit tensor operator $U^{(\lambda)}$,

$$P_{AB}^{qd} = \frac{2\pi}{\hbar}\frac{1}{\kappa^2}\frac{e^4}{R^8}\frac{1}{(2J+1)(2J'+1)}\left[(1-\sigma_2)^2\left\langle r^2\right\rangle^2\left\langle f\left\|c^2\right\|f\right\rangle^2\left\langle J\left\|U^{(2)}\right\|J'\right\rangle^2\right]$$
$$\times \left[\sum_q \left|\left\langle 00\left|M_q^1(B)\right|0n\right\rangle\right|^2\right]\rho_E, \tag{7}$$

for the electric quadrupole–electric dipole interaction, where σ_2 is the screening factor due to the outer filled $5s^2$ and $5p^6$ shells of the lanthanide ion [15], $\langle r^2\rangle$ is the expectation value of r^2 for the 4f orbital, and the reduced matrix element $\langle f||c^2||f\rangle^2 = 28/15$,

$$P_{AB}^{dq} = \frac{2\pi}{\hbar}\frac{1}{\kappa^2}\frac{e^4}{R^8}\frac{1}{(2J+1)(2J'+1)}\left[\sum_{\lambda=2,4,6}\Omega_\lambda^{\mathrm{ed}}\left\langle J\left\|U^{(\lambda)}\right\|J'\right\rangle\right]$$
$$\times \left[\sum_q \left|\left\langle 00\left|M_q^2(B)\right|0n\right\rangle\right|^2\right]\rho_E, \tag{8}$$

for the electric dipole–electric quadrupole interaction and

$$P_{AB}^{qq} = \frac{2\pi}{\hbar}\frac{1}{\kappa^2}\left(\frac{14}{5}\right)\frac{e^4}{R^{10}}\frac{1}{(2J+1)(2J'+1)}\left[(1-\sigma_2)^2\left\langle r^2\right\rangle^2\left\langle f\left\|c^2\right\|f\right\rangle^2\left\langle J\left\|U^{(2)}\right\|J'\right\rangle^2\right]$$
$$\times \left[\sum_q \left|\left\langle 00\left|M_q^2(B)\right|0n\right\rangle\right|^2\right]\rho_E \tag{9}$$

for the electric quadrupole–electric quadrupole interaction.

3. Modelling of OH vibration

For the squared transition matrix elements of OH (centre B) in equations (6)–(9), Stavola and Dexter [7] estimated the values for the $|00\rangle \rightarrow |01\rangle$ transition in condensed matter from the experimental oscillator strength of the OH fundamental absorption band. In this work, however, we evaluated them analytically by developing a reasonable model for the OH vibration in solution. From equation (3), the transition matrix element may be expressed as

$$\left\langle 00\left|M_q^k(B)\right|0n\right\rangle = \langle 0|\int \rho(\vec{r},\vec{x})r^k C_q^k(\theta,\phi)\,\mathrm{d}\vec{r}|n\rangle - \langle 0|\sum_L Z_L x_L^k C_q^k(\theta_L,\phi_L)|n\rangle \tag{10}$$

where $\rho(\vec{r},\vec{x})$ is the probability density of finding an electron at position $\vec{r}$ in the nuclear configuration $\vec{x}$. The evaluation of the first matrix element in equation (10) is usually difficult because it involves integrals over both the electron and nuclear coordinates. However, it is possible to formulate a model for the OH vibration, in which the first matrix element may be neglected and the second greatly simplified, as shown in the following. We assume that the hydrogen atom is bonded to an infinitely massive atom which represents the oxygen atom, and is constrained to move along the z axis of the coordinate system B with the equilibrium position at the origin ($z = 0$). The massive atom is located at (0, 0, z_0), with z_0 equal to the equilibrium OH separation. In this way, the electronic density $\rho(\vec{r},\vec{x})$ in (10) may be

assumed to be independent of $\vec{x}$, that is, $\rho(\vec{r},\vec{x}) \approx \rho(\vec{r},z_0)$, since the electron charge cloud is mainly located around the immobile massive atom. This is because oxygen has a much larger electronegativity than hydrogen. Certainly, this assumption is not applicable to the CH vibration. The first matrix element in (10) is then zero if $n \neq 0$ due to orthogonality of the vibrational wavefunctions. In addition, with the atomic number of hydrogen, $Z_L = 1$, and the polar coordinates, $x_L = z$, $\theta_L = 0°$ or 180°, and $\phi_L = 0°$, the second matrix element, after some mathematical manipulations, is simplified to

$$\langle 0|\sum_L Z_L x_L^k C_q^k(\theta_L,\phi_L)|n\rangle = \delta_{q,0}\langle 0|z^k|n\rangle \tag{11}$$

where z describes the departure of the hydrogen atom from its equilibrium position. In the following, we will denote $\langle 0|z^k|n\rangle$ by $z_{0n}^{(k)}$ for brevity. In order to evaluate $z_{0n}^{(k)}$, a Morse potential has been employed for the OH vibration,

$$V(z) = D[1-\exp(-az)], \tag{12}$$

where the parameters D (in cm^{-1}) and a (in $\mathrm{Å}^{-1}$) are related to the spectroscopic vibrational constants, namely the fundamental frequency ω_e (in cm^{-1}) and the anharmonic constant χ_e, by [16]

$$D = \omega_e^2/(4\omega_e\chi_e) \qquad \text{and} \qquad a = 0.2436\,(\mu\omega_e\chi_e)^{1/2}$$

in which, $\mu = 1$ amu, is the reduced mass of OH. With eigenfunctions of the Morse potential, the analytical expressions for $z_{0n}^{(k)}$ $(k = 1, 2)$ can be written as [17]

$$z_{0n}^{(1)} = \frac{(-1)^{n+1}}{an(k-n-1)}\left(n!\frac{\Gamma(k-n)}{\Gamma(k)}(k-1)(k-2n-1)\right)^{1/2},$$

$$z_{0n}^{(2)} = \frac{2\ln(k)}{a}M_{0n}^{(1)} + \frac{2}{a^2}(-1)^{n-1}\left(\frac{1}{n!}\frac{\Gamma(k)}{\Gamma(k-n)}(k-1)(k-2n-1)\right)^{1/2} \times \frac{\Gamma(k-n-1)}{\Gamma(k)}(n-1)![\psi(1)-\psi(n)-\psi(k-n-1)],$$

where $k = \omega_e/(\omega_e\chi_e)$, $\Gamma(x)$ is the gamma function and $\psi(x) = \Gamma'(x)/\Gamma(x)$ is the digamma function. In the present study on the ET, involving the $^4\mathrm{I}_{13/2} \rightarrow {}^4\mathrm{I}_{15/2}$ transition of Er^{3+} and the first overtone $|00\rangle \rightarrow |02\rangle$ transition of OH, only the squared matrix elements with $n = 2$ are needed. They are given by

$$\left|z_{02}^{(1)}\right|^2 = \frac{1}{a^2}\frac{(k-5)}{2(k-2)}\frac{1}{(k-3)^2},$$

$$\left|z_{02}^{(2)}\right|^2 = \frac{2\ln(k)}{a}M_{02}^{(1)} + \frac{1}{a^2}\left(\frac{2(k-5)}{(k-2)(k-3)^2}\right)^{1/2}[1+\psi(k-3)].$$

With the typical values, $\omega_e = 3400\ \mathrm{cm}^{-1}$ and $\chi_e = 0.025$, for the OH fundamental frequency and the anharmonic constant in solution [18–21], respectively, we obtain

$$\left|z_{02}^{(1)}\right|^2 = \langle 0\,|z|\,2\rangle^2 = 2.25\times 10^{-4}a_0^2 \qquad \text{and} \qquad \left|z_{02}^{(2)}\right|^2 = \left\langle 0\left|z^2\right|2\right\rangle^2 = 4.96\times 10^{-4}a_0^2, \tag{13}$$

where a_0 is the Bohr radius. The values for the two squared matrix elements in equation (13) enable us to compare the relative importance of the various ET mechanisms as described in equations (6)–(9). Note that in the limit $\chi_e \rightarrow 0$, the two squared matrix elements would reach the harmonic values, i.e. $|z_{02}^{(1)}|^2 = 0$ and $|z_{02}^{(2)}|^2 = 5.59\times 10^{-4}a_0^2$.

4. Results and discussion

4.1. ET rates for a single Er^{3+} and OH pair

In order to calculate the ET rate from LaF_3:Er^{3+} nanoparticles to OH in solution, the various quantities appearing in (6)–(9) need to be evaluated. The reduced matrix elements of the unit tensors $U^{(\lambda)}$ may be taken from the work by Weber [13], in which $\langle {}^4I_{13/2}||U^{(\lambda)}||{}^4I_{15/2}\rangle = 0.0188$, 0.1176, and 1.4617 for $\lambda = 2$, 4 and 6, respectively. The intensity parameters $\Omega_\lambda^{\rm ed}$ were approximated by the experimentally determined Judd–Ofelt (JO) parameters for the LaF_3:Er^{3+} crystal [13], and are given by $\Omega_2^{\rm ed} = 2.71 \times 10^{-4} a_0^2$, $\Omega_4^{\rm ed} = 0.69 \times 10^{-4} a_0^2$, and $\Omega_6^{\rm ed} = 1.60 \times 10^{-4} a_0^2$. We supposed here that the dynamic-coupling contributions, which are contained in the experimentally determined JO intensity parameters, are not important for the ${}^4I_{13/2} \rightarrow {}^4I_{15/2}$ transition. This is because the dynamic-coupling mechanism mainly influences transitions with larger $\langle J||U^{(2)}||J'\rangle$ values for $\lambda = 2$ than those for $\lambda = 4$ and 6, whereas the ${}^4I_{13/2} \rightarrow {}^4I_{15/2}$ transition mainly depends on the element with $\lambda = 6$. In addition, the values of the radial integral $\langle r^2\rangle$ and the screening factor σ_2 were taken from a relativistic Hartree–Fock calculation with $\langle r^2\rangle = 0.710 a_0^2$ and $\sigma_2 = 0.541$, respectively [22]. The dielectric constant for the LaF_3 crystal was applied with $\kappa = 1.58$ [23].

For the overlap integral ρ_E between the ${}^4I_{13/2} \rightarrow {}^4I_{15/2}$ emission band of Er^{3+} in LaF_3:Er^{3+} nanoparticles and the first overtone $|00\rangle \rightarrow |02\rangle$ band of OH in solution, only a crude estimate has been made. From the definition of ρ_E in equation (5), the line shape functions for the transitions from the ${}^4I_{13/2}$ manifold to each of the 16 components of the ${}^4I_{15/2}$ manifold have unit area, and thus the total area for the entire ${}^4I_{13/2} \rightarrow {}^4I_{15/2}$ emission band is 16. At room temperature, the ${}^4I_{13/2} \rightarrow {}^4I_{15/2}$ emission of the LaF_3:Er^{3+} nanoparticle was assumed to give a Gaussian shaped band peaked at 6540 cm^{-1} (1.53 μm) with the full width at half maximum (FWHM) of about 300 cm^{-1} [2]. For the first overtone $|00\rangle \rightarrow |02\rangle$ transition of OH, a Gaussian band was also used with a FWHM of about 300 cm^{-1}. This FWHM value is a little larger than the typical value (250 cm^{-1}) for the OH fundamental absorption band in solution [24]. Moreover, considering the wide variety of OH environments in solution [25], a resonant ET from Er^{3+} (${}^4I_{13/2} \rightarrow {}^4I_{15/2}$) to OH ($|00\rangle \rightarrow |02\rangle$) has been adopted. Then, for such two Gaussian bands, the overlap integral ρ_E has been estimated to be of the order of 10^{-2} cm^{-1}.

Substituting the values for the various quantities into equations (6)–(9), we have the following expressions for the ET rates from a given Er^{3+} ion in the LaF_3 nanoparticle to one of the OH groups in solution:

$$P_{AB}^{dd} = 3.77 \times 10^{10} \left(\frac{a_0}{R}\right)^6 \ {\rm s}^{-1}, \tag{14a}$$

$$P_{AB}^{dq} = 1.24 \times 10^{11} \left(\frac{a_0}{R}\right)^8 \ {\rm s}^{-1}, \tag{14b}$$

$$P_{AB}^{qd} = 8.53 \times 10^{11} \left(\frac{a_0}{R}\right)^8 \ {\rm s}^{-1}, \tag{14c}$$

$$P_{AB}^{qq} = 5.29 \times 10^{12} \left(\frac{a_0}{R}\right)^{10} \ {\rm s}^{-1}, \tag{14d}$$

which show that the dipole–quadrupole interaction is much smaller than the quadrupole–dipole interaction, though with the same $1/R^8$ dependence. From the above expressions, the R dependence of the ET rates within the range of $R = 2$–30 Å is shown in figure 2, together with that of the total ET rate

$$P_{AB}^{\rm tot} = P_{AB}^{dd} + P_{AB}^{dq} + P_{AB}^{qd} + P_{AB}^{qq}, \tag{15}$$

while the radiative ${}^4I_{13/2} \rightarrow {}^4I_{15/2}$ transition rate constant $k_{\rm R} = 1/\tau_{\rm R}$ is denoted by a horizontal line, where $\tau_{\rm R} = 13$ ms is the natural radiative lifetime of the ${}^4I_{13/2}$ manifold [13], that is, a

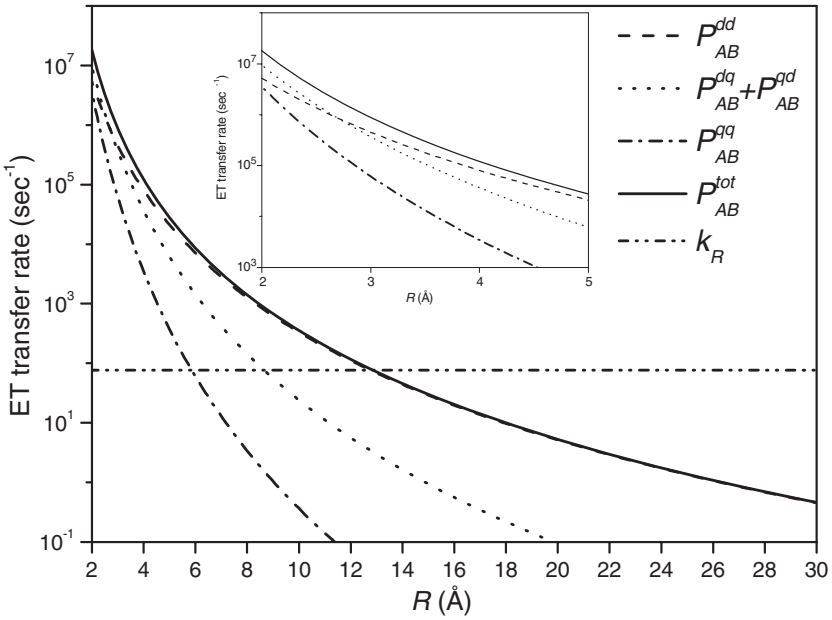

Figure 2. Dependence of ET rates on the separation R between an Er^{3+} ion in the LaF_3 nanoparticle and an OH group in the solution within the range of $R = 2$–30 Å. The radiative $^4I_{13/2} \rightarrow {}^4I_{15/2}$ transition rate constant $k_R = 1/\tau_R$ ($\tau_R = 13$ ms) is also included by a horizontal line. The inset shows the dependence on the separation R from 2 to 5 Å.

lifetime that would be measured in the absence of any ET between Er^{3+} ions inside the LaF_3 nanoparticle. From the inset of figure 2, we can see that, for a separation of ∼2.7 Å, the quadrupole–dipole plus dipole–quadrupole interactions are comparable in magnitude to the dipole–dipole interaction in quenching the $^4I_{13/2} \rightarrow {}^4I_{15/2}$ luminescence. They are operative up to a separation of 6 Å, and then the dipole–dipole interaction dominates the total quenching for longer distances. The decrease of the total quenching rate $P^{\rm tot}_{AB}$ with increasing R is steeper for $R \leqslant 5$ Å. For example, an increase of R from 2.5 to 5 Å would cause a reduction of two orders of magnitude in the total quenching rate. The quadrupole–quadrupole interaction can be readily neglected for a separation larger than 3 Å. The total quenching rate $P^{\rm tot}_{AB}$ is comparable to the radiative transition rate constant k_R at $R = 13$ Å, and becomes negligible in quenching the $^4I_{13/2} \rightarrow {}^4I_{15/2}$ luminescence when the separation is larger than 20 Å.

It is worth noting that besides the aforementioned quenching processes involving a single Er^{3+} ($^4I_{13/2} \rightarrow {}^4I_{15/2}$) and OH (00 → 02) pair another kind of quenching, called cooperative quenching [26], could be operative here. This quenching, first predicted by Dexter [27] and recently identified experimentally by Basiev *et al* [28], takes place in a simultaneous ET from a single Er^{3+} ($^4I_{13/2} \rightarrow {}^4I_{15/2}$) ion to two OH (00 → 01) fundamental vibrations, in view of the good resonance in the transition energies. Along the lines of Kushida [8], the expressions for the ET rates for these processes, which are due to (Er^{3+}, OH)–(Er^{3+}, OH) interactions, have been derived [29], and for the largest (dipole, dipole)–(dipole, dipole) (dd–dd) contribution, it is given by

$$P^{dd-dd}_{AB-AC} = 1.04 \times 10^{12} \left(\frac{a_0}{R}\right)^{12} \ {\rm s}^{-1}$$

where the two (Er^{3+}, OH) distances R were taken to be the same. For a distance $R = 2.5$ Å, which is about the nearest Er^{3+}–OH separation [30] in the system under consideration, P^{dd-dd}_{AB-AC}

was estimated to be 8.4×10^5 s^{-1}, a value three orders of magnitude smaller than P_{AB}^{tot} (8.4×10^8 s^{-1}) from equation (15). The contributions of the dd–dq (or dq–dd) and dq–dq processes can also be estimated. The results show that these contributions are respectively two and ten orders of magnitude smaller than that due to the dd–dd mechanism for the above separation. Therefore, the contribution from cooperative quenching is negligible compared to that due to the single (Er^{3+}, OH) pair interaction, and is omitted in the subsequent sections.

4.2. ET rates between LaF_3:Er^{3+} nanoparticles and OH groups in solution

The observed $^4I_{13/2} \rightarrow {}^4I_{15/2}$ luminescence for a given LaF_3:Er^{3+} nanoparticle consists of contributions from all the Er^{3+} ions in the nanoparticle; for each Er^{3+} ion, the luminescence quenching results from interaction with all the OH groups in solution. From figure 2, one can see that most of the quenching is through interactions with the OH groups at/near the particle surface. To consider the different quenching rates for Er^{3+} ions in different locations, the nanoparticle, which is assumed to be spherical in shape, is divided into a number of spherical shells of equal volume as in [3]. This is to ensure equal weight for Er^{3+} in each shell, with the assumption of a homogeneous Er^{3+} distribution in the nanoparticle.

Consider now the case in which the concentration of Er^{3+} in the LaF_3 nanoparticle is so small that the self-quenching of luminescence through ET between Er^{3+} ions inside the nanoparticle is negligible, like for example the upconversion ET between two excited $^4I_{13/2}$ states and the migration of the $^4I_{13/2}$ excitation to an impurity inside the particle or at the surface (i.e. diffusion to energy sinks). For a given Er^{3+} in shell i, the $^4I_{13/2} \rightarrow {}^4I_{15/2}$ luminescent decay rate constant k_i can be expressed as

$$k_i = k_{qi} + k_{\text{R}}, \tag{16}$$

where k_{qi} is the quenching rate constant due to the interaction with all the OH groups outside the nanoparticle, and k_{R} is the aforementioned radiative rate constant of the $^4I_{13/2} \rightarrow {}^4I_{15/2}$ transition, which is the same for Er^{3+} in all shells. The quenching rate constant k_{qi} in equation (16) may be calculated by using

$$k_{qi} = \rho_{\text{OH}} \int_V P_{AB}^{\text{tot}}\,\text{d}V = \rho_{\text{OH}} \left(\int_{V_{\text{I}}} P_{AB}^{\text{tot}}\,\text{d}V + \int_{V_{\text{II}}} P_{AB}^{\text{tot}}\,\text{d}V + \int_{V_{\text{III}}} P_{AB}^{\text{tot}}\,\text{d}V \right), \tag{17}$$

where P_{AB}^{tot} is the total quenching rate constant for a single (Er^{3+}, OH) pair as expressed in equations (14) and (15), and ρ_{OH} is the concentration of OH in solution, which was also assumed to be homogeneously distributed. In the second step of equation (17), the integration volume V is divided into three spherical domains (I, II and III) with the Er^{3+} (in shell i) at the centre, as also shown in figure 3. In this figure, the spherical nanoparticle with radius R is represented by the shaded area, the distance between the centres of shell i and the nanoparticle is denoted by R_i, and the partition of the integration volume is indicated by the solid lines. The first spherical domain (I) with radius $R - R_i$, is totally inside the particle without any OH present, and consequently will not contribute to k_{qi}. The second domain (II) that is a spherical shell with inner and outer radii of $R - R_i$ and $R + R_i$, respectively, is partially inside the particle without quenching and partially outside with quenching. The third one (III) with radius extending from $R + R_i$ to infinite, lies totally outside the particle with full quenching. A detailed description of the integration in these three domains may be found in [3]. Dividing each of the nanoparticles with radii $R_0 = 1$–10 nm into 100 shells, we calculated the quenching rate constant k_{qi} for one Er^{3+} in each shell by numerical integration. The results are shown in figure 4(a). The OH concentration in pure water, $\rho_0 = 6.7 \times 10^{-2}$ Å^{-3}, has been used for ρ_{OH} in equation (17). In the integration, we have taken a distance of 2.5 Å, which is about the nearest

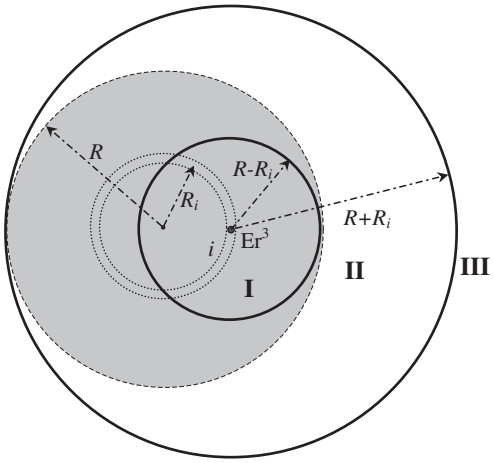

Figure 3. Schematic representation of a spherical nanoparticle by shaded area, and of the partition of the integration volume around a given Er^{3+} in shell i into three spherical domains (I, II and III) indicated by the solid lines.

La–F separation in the LaF_3 crystal [30], as the minimum cut-off distance between Er^{3+} at the outmost shell and OH at/near the surface. This is to remove the abnormally high k_{qi} values that would result from unrealistically small R values (see equations (14*a*)–(14*d*)). In figure 4(a), the radiative transition rate constant $k_R = 1/\tau_R$ ($\tau_R = 13$ ms) is indicated by a horizontal line for comparison. As implied by equation (17), if the OH concentration ρ_{OH} were reduced by orders of magnitude, the quenching rate constants k_{qi} would scale down accordingly. As a specific example, we consider the LaF_3:Er^{3+} nanoparticle with radius $R_0 = 5$ nm. The quenching rate constants k_{qi} ($i = 1$–100) with $\rho_{OH} = \rho_0$, $\rho_0 \times 10^{-1}$, $\rho_0 \times 10^{-2}$, $\rho_0 \times 10^{-3}$ and $\rho_0 \times 10^{-4}$, are shown in figure 4(b). It is interesting to see that, when $\rho_{OH} \leqslant \rho_0 \times 10^{-3}$, the $^4I_{13/2} \rightarrow {}^4I_{15/2}$ luminescence quenching of the LaF_3:Er^{3+} nanoparticle by the OH is small. It should be noted that if an Er^{3+} ion were exposed directly to solution the quenching rate constant by OH would be even larger than that for an Er^{3+} ion at the surface of a LaF_3 nanoparticle dissolved in the solution. This is because the Er^{3+} ion at the surface is only partially exposed to the liquid environment.

4.3. Effective $^4I_{13/2} \rightarrow {}^4I_{15/2}$ luminescence lifetimes for LaF_3:Er^{3+} nanoparticles

Due to the different quenching rates for the Er^{3+} ions in the different shells of a nanoparticle, the observed $^4I_{13/2} \rightarrow {}^4I_{15/2}$ luminescence decay is multi-exponential in character. For this reason, we calculated the effective decay time τ_{eff} of the luminescence by [31]

$$\tau_{eff} = \frac{\int_0^\infty t\, I(t)\, dt}{\int_0^\infty I(t)\, dt} = \frac{\sum_{i=1}^n A_i/k_i^2}{\sum_{i=1}^n A_i/k_i}, \tag{18}$$

where $I(t)$ is the luminescence intensity at time t, k_i is the decay rate constant for the Er^{3+} in shell i as expressed in equation (16) and $A_i = 1/n = 0.01$. The effective decay times for the LaF_3:Er^{3+} nanoparticles with radii $R_0 = 1$–10 nm and with various OH concentrations in solution are presented in figure 5. Figure 5(a) shows the results obtained with the natural radiative life time $\tau_R = 13$ ms. This corresponds to the case in which the $^4I_{13/2} \rightarrow {}^4I_{15/2}$ luminescence self-quenching due to ET between Er^{3+} ions is absent.

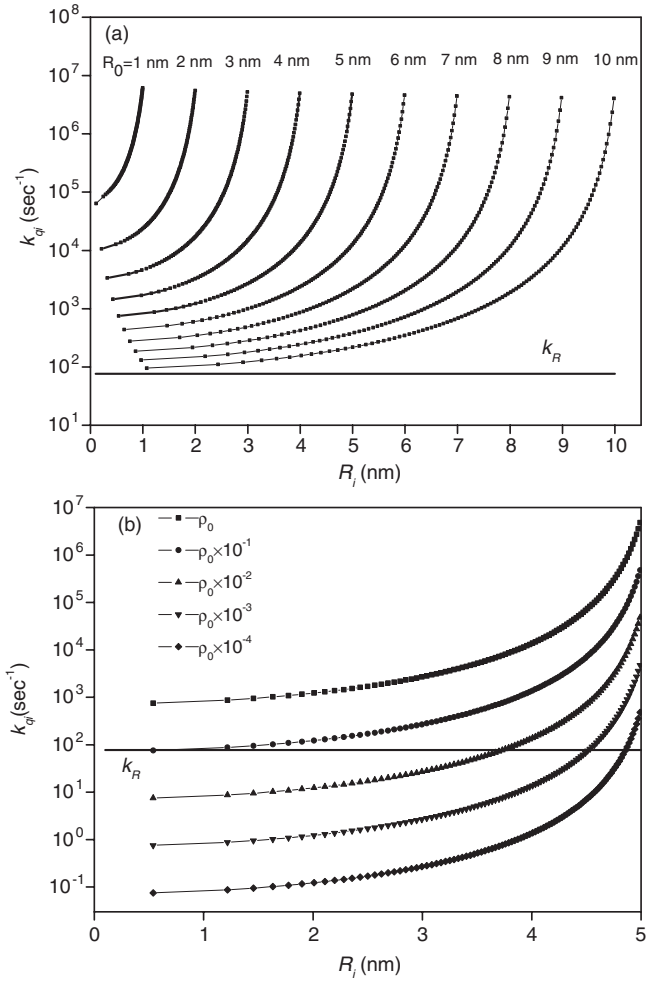

Figure 4. (a) The $^4I_{13/2} \rightarrow {}^4I_{15/2}$ luminescence quenching rate constant k_{qi} for an Er^{3+} ion in shell i (i = 1–100) of the LaF_3:Er^{3+} nanoparticle with radii R_0 = 1–10 nm in pure water. (b) k_{qi} (i = 1–100) for a LaF_3:Er^{3+} nanoparticle with R_0 = 5 nm and the OH concentration $\rho_{OH} = \rho_0$, $\rho_0 \times 10^{-1}$, $\rho_0 \times 10^{-2}$, $\rho_0 \times 10^{-3}$ and $\rho_0 \times 10^{-4}$, where ρ_0 is the OH concentration in pure water. The coordinate R_i represents the distance of shell i from the centre of the nanoparticle. The radiative $^4I_{13/2} \rightarrow {}^4I_{15/2}$ transition rate constant $k_R = 1/\tau_R$ (τ_R = 13 ms) is also plotted by the horizontal line.

When the Er^{3+} concentration in the LaF_3 nanoparticle is increased self-quenching occurs, and becomes important and even dominant compared to the quenching by OH. In these cases, the radiative constant k_R in equation (16) should be replaced by $k_R + k_Q$, where k_Q is the self-quenching rate constant. For LaF_3 nanoparticles with an average diameter of 6.3 nm and with the atomic Er^{3+} concentrations of 1%, 2% and 5%, the experimental (fitted) values of k_Q are 2.02×10^3, 2.93×10^3 and 4.15×10^3 s^{-1}, respectively [3]. A plot of k_Q versus Er^{3+} concentrations is presented in figure 6, which shows a linear relationship, corresponding to the fast diffusion case, in which the migration of the $^4I_{13/2}$ excitation between Er^{3+} ions is faster than the other self-quenching processes [32]. Figures 5(b)–(d) depict the calculated effective decay times τ_{eff} for the LaF_3:Er^{3+} nanoparticles with Er^{3+} concentrations

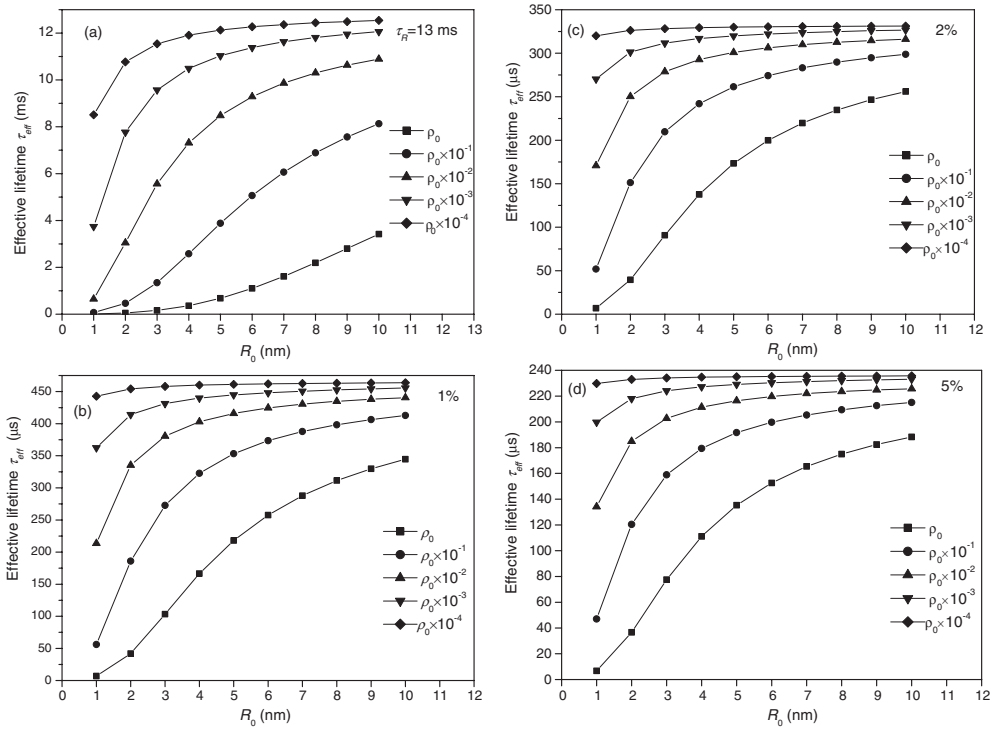

Figure 5. The effective decay time τ_{eff} of the $^4I_{13/2} \rightarrow {}^4I_{15/2}$ luminescence for LaF_3:Er^{3+} nanoparticle with radii $R_0 = 1$–10 nm and OH concentration $\rho_{\text{OH}} = \rho_0$, $\rho_0 \times 10^{-1}$, $\rho_0 \times 10^{-2}$, $\rho_0 \times 10^{-3}$ and $\rho_0 \times 10^{-4}$, where ρ_0 is the OH concentration in pure water. The $\tau_{\text{R}} = 13$ ms in panel (a) refers to the case without ET between Er^{3+} ions inside the nanoparticle, whereas the concentrations 1%, 2% and 5% in panels (b), (c) and (d) refer to the cases where ET exists between Er^{3+} ions.

of 1%, 2% and 5%, respectively. The corresponding experimental k_{Q} values, which are independent of particle sizes, have been used in the calculations. Furthermore, the ranges of τ_{eff} for a LaF_3:Er^{3+} nanoparticle with diameter of 6.3 nm and with the OH concentration $\rho_{\text{OH}} = \rho_0 \times 10^{-2}$–$\rho_0 \times 10^{-3}$, were calculated and are listed in the second column of table 1. The experimental values in the third column were obtained from table 4 of [3] for LaF_3:Er^{3+} (1%, 2%, 5%) nanoparticles of the above size dissolved in the organic solvent. A comparison between the calculated and experimental τ_{eff} values indicates interestingly that the concentration of the OH group in the organic solvent is within the range of $\rho_0 \times 10^{-3}$–$\rho_0 \times 10^{-2}$, confirming the quenching role of the residual water in the solvent [3].

We also investigated briefly the case of the LaF_3:Er^{3+} core–shell nanoparticle in which an Er^{3+} doped LaF_3 core is surrounded by an undoped LaF_3 shell. Since the Er^{3+} ions at the outmost part of the nanoparticle experience the largest luminescence quenching by the outside OH groups, it is expected that the effective decay time τ_{eff} will increase with increase in the undoped shell volume. The last column of table 1 lists the τ_{eff} values for a LaF_3:Er^{3+} core–shell nanoparticle with a diameter of 6.3 nm, where the undoped LaF_3 shell accounts for 1/10 of the whole particle volume, and with the OH concentration $\rho_{\text{OH}} = \rho_0 \times 10^{-2}$–$\rho_0 \times 10^{-3}$. A comparison with the corresponding LaF_3:Er^{3+} values in the second column shows a small but apparent increase of τ_{eff} values when the core is covered by an undoped LaF_3 shell.

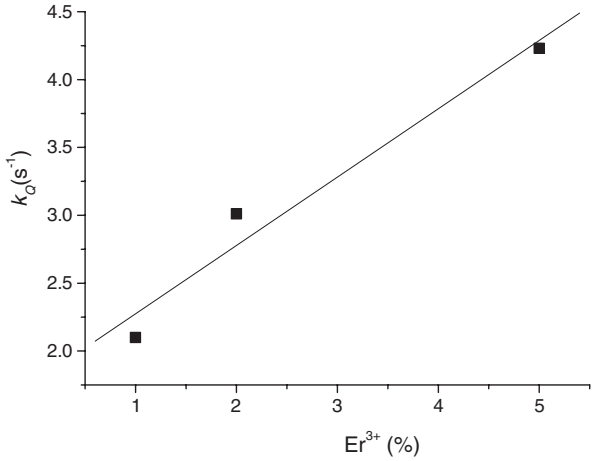

Figure 6. The self-quenching rate constants k_Q versus Er^{3+} atomic concentrations for the LaF_3 nanoparticles with an average diameter of 6.3 nm.

Table 1. The calculated effective decay time τ_{eff} of the $^4I_{13/2} \rightarrow {}^4I_{15/2}$ luminescence for the LaF_3:Er^{3+} nanoparticle with a diameter of 6.3 nm and an OH concentration $\rho_{OH} = \rho_0 \times 10^{-2}$–$\rho_0 \times 10^{-3}$, where ρ_0 is the OH concentration in pure water. The experimental τ_{eff} values were obtained from [3].

	τ_{eff}		τ_{eff} (core–shell)
	Calc.	Expt.	Calc.
LaF_3:Er^{3+}[a]	5.87–9.75 ms	—	5.88–9.80 ms
LaF_3:Er^{3+} (1%)	385–433 μs	404 μs	389–445 μs
LaF_3:Er^{3+} (2%)	282–313 μs	292 μs	285–321 μs
LaF_3:Er^{3+} (5%)	204–226 μs	212 μs	208–230 μs

[a] The luminescence self-quenching due to ET between Er^{3+} ions is absent.

5. Conclusions

We have performed theoretical calculations for the ET processes involving the $^4I_{13/2} \rightarrow {}^4I_{15/2}$ transition of Er^{3+} in the LaF_3 nanoparticle and the first overtone transition of OH in solution. The required OH transition matrix elements have been obtained by developing a model for the OH vibration in solution with the use of a Morse potential. Dependences of ET rates for a single (Er^{3+}, OH) pair of various multipole–multipole mechanisms on their separation have been investigated, showing that the dipole–dipole mechanism becomes dominant when the separation is larger than 6 Å. The ET rates from the Er^{3+} ions in different places inside nanoparticles with different size to all the OH groups in solution with various concentrations have been calculated. The effective decay time of the multi-exponential $^4I_{13/2} \rightarrow {}^4I_{15/2}$ luminescence of the LaF_3:Er^{3+} particle in solution has been systematically studied with respect to changes in size of the particle, Er^{3+} concentration in the nanoparticle, and OH concentration in solution. The experimental results are satisfactorily accounted for by the calculations [3]. Finally, a brief investigation for the case of the LaF_3:Er^{3+} core–shell nanoparticle has been made.

It should be noted that the ET from Er^{3+} to OH would possibly require the annihilation of a few phonons from the LaF_3 host, and an effective repopulation of the $^4I_{13/2}$ through back-transfer from OH would be considerably attenuated by the extremely short lifetime of the OH overtone. Moreover, in the calculation we have assumed that the local environments of Er^{3+} on the surface of the LaF_3 nanoparticle are the same as those of Er^{3+} in the bulk, and thus the radiative lifetimes τ_R are equal in the two cases. It has been shown recently [33] that the surface ions experience a less symmetric CF than the ion in the bulk, and the surface effects can be very effectively reduced by forming core–shell particles. In addition, lanthanide-doped nanoparticles of different sizes in a solvent show different luminescence lifetimes due to the different effective refractive indices [34]. These effects on the results of the present study are expected to be small in view of the small difference of the refractive indices between the LaF_3 (1.58) and the organic solvent (for example, 1.42 for CH_2Cl_2). Finally, the exchange Coulomb interaction between Er^{3+} and OH has not been taken into account. Since the dipole–dipole ET mechanism is allowed in the present case, the inclusion of exchange effects would not materially change the results.

Acknowledgments

The authors would like to acknowledge financial support from Fondazione CARIPLO-n.Prot.0018524 and FIRB RBNE03S7XZ 'SYNERGY'. Helpful comments by the referees are appreciated.

References

[1] Hebbink G A, Stouwdam J W, Reinhoudt D N and van Veggel F C J M 2002 *Adv. Mater.* **14** 1147
[2] Stouwdam J W and van Veggel F C J M 2002 *Nano Lett.* **2** 733
[3] Stouwdam J W, Hebbink G A, Huskens J and van Veggel F C J M 2003 *Chem. Mater.* **15** 4604
[4] Heer S, Lehmann O, Haase M and Güdal H U 2003 *Angew. Chem. Int. Edn* **42** 3179
[5] Heer S, Kömpe K, Güdal H U and Haase M 2004 *Adv. Mater.* **16** 2102
[6] Terpilovskii D N 1968 *Opt. Spektrosk.* **24** 313
[7] Stavola M and Dexter D L 1979 *Phys. Rev.* B **20** 1867
[8] Kushida T 1973 *J. Phys. Soc. Japan* **34** 1318
[9] Watts R K 1975 *Optical Properties of Ions in Solids* ed B Di Bartolo (New York: Plenum) p 307
[10] Chua M, Xia S and Tanner P A 2003 *J. Phys.: Condens. Matter* **15** 7423
[11] Förster T 1948 *Ann. Phys., Lpz.* **2** 55
[12] Dexter D L 1953 *J. Chem. Phys.* **21** 836
[13] Weber M J 1967 *Phys. Rev.* **157** 262
[14] Malta O L and Carlos L D 2003 *Quim. Nova.* **26** 889
[15] Faucher M and Garcia D 1982 *Phys. Rev.* B **26** 5421
[16] Herzberg G 1950 *Molecular Spectra and Molecular Structure I. Spectra of Diatomic Molecules* (Princeton, NJ: Van Nostrand-Reinhold)
[17] Gallas J A 1980 *Phys. Rev.* A **21** 18290
[18] Luque J and Crosley D R 1998 *J. Chem. Phys.* **109** 439
[19] Weibl J D, Jackels C F and Swofford R L 2002 *J. Chem. Phys.* **117** 4245
[20] Bünzli J C G 2005 *Spectroscopic Properties of Rare Earths in Optical Materials* ed G Liu and B Jacquier (Tsinghua, China: Tsinghua University Press) p 462
[21] Schofield D P, Kjaergaard H G, Matthews J and Sinha A 2005 *J. Chem. Phys.* **123** 134318
[22] Edvardsson S and Klintenberg M 1999 *Mater. Sci. Forum* **315** 407
[23] Hass G, Ramsey J B and Thun R 1959 *J. Opt. Soc. Am.* **49** 407
[24] Wyss H R and Falk M 1970 *Can. J. Chem.* **48** 607
[25] Beeby A, Clarkson I M, Dickins R S, Faulkner S, Parker D, Royle L, de Sousa A S, Williams J A G and Woods M 1999 *J. Chem. Soc. Perkin Trans.* **2** 493
[26] Auzel F 2004 *Chem. Rev.* **104** 139

[27] Dexter D L 1957 *Phys. Rev.* **108** 630
[28] Basiev T T, Doroshenko M E and Osiko V V 2000 *JETP Lett.* **71** 8
[29] Ning L 2006 unpublished results
[30] Cheetham A K, Fender B E F, Fuess H and Wright A F 1976 *Acta Crystallogr.* B **32** 94
[31] Nakazawa E 1999 *Phosphor Handbook* ed S Shionoya and W M Yen (Boca Raton, FL: CRC Press) p 93
[32] Auzel F 1987 *Spectroscopy of Solid-State Laser-Type Materials* ed B Di Bartolo (New York: Plenum) p 293
[33] Sudarsan V, van Veggel F C J M, Herring R A and Raudsepp M 2005 *J. Mater. Chem.* **15** 1332
[34] Meltzer R S, Feofilov S P, Tissure B and Yuan H B 1999 *Phys. Rev.* B **60** 14012